Nonadiabatic Hydrogen Dissociation on Copper Nanoclusters

Robert A. Hoyt,[†] Matthew M. Montemore,[‡] and Efthimios Kaxiras[*,†,‡]

Department of Physics, Harvard University, Cambridge, MA 02138, USA, and John A. Paulson School of Engineering and Applied Sciences, Harvard University, Cambridge, MA 02138, USA

E-mail: kaxiras@physics.harvard.edu

[*]To whom correspondence should be addressed
[†]Harvard University Department of Physics
[‡]Harvard University John A. Paulson School of Engineering and Applied Sciences

Abstract

Copper surfaces exhibit high catalytic selectivity but have poor hydrogen dissociation kinetics, so we consider icosahedral Cu_{13} nanoclusters to understand how nanoscale structure might improve catalytic prospects. We find that the spin state is a surprisingly import design consideration. Cu_{13} clusters have large magnetic moments due to finite size and symmetry effects and exhibit magnetization-dependent catalytic behavior. The most favorable transition state for hydrogen dissociation has a lower activation energy than on single-crystal copper surfaces, but requires a magnetization switch from $5\,\mu_B$ to $3\,\mu_B$. Without this switch the activation energy is *higher* than on single-crystal surfaces. Weak spin-orbit coupling hinders this switch, decreasing the kinetic rate of hydrogen dissociation by a factor of 16. We consider strategies to facilitate magnetization switches through optical excitations, substitution, charge states, and co-catalysts; these considerations demonstrate how control of magnetic properties could improve catalytic performance.

Graphical TOC Entry

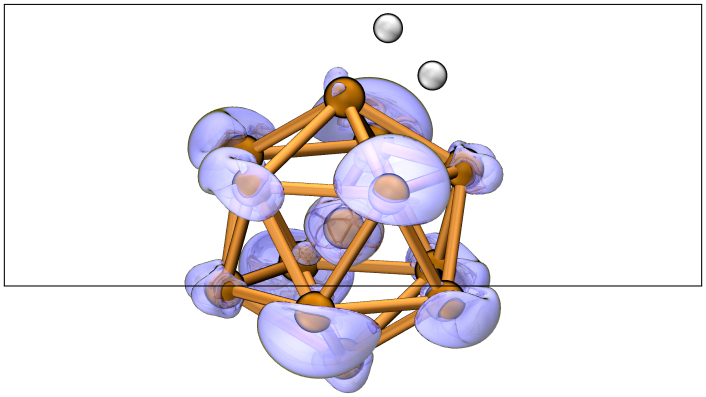

Transition metal catalysts are ubiquitous in industrial applications of heterogeneous catalysis. Their wide-ranging applications, from catalytic cracking to highly selective hydrogenation, are derived from the large variety of electronic properties across the periodic table. These intrinsic properties are further modified through structural and compositional changes induced by alloying, oxidation, surface structure modification, metal-support interactions, and promotors, providing enormous flexibility in catalytic design. In recent years, progress in nanotechnology has introduced the nanocluster size and geometry as new catalyst design parameters.[1] As the nanocluster diameter approaches 1 nm and below, finite size effects can become especially pronounced and produce surprising effects like a discontinuous change in catalytic activity upon the addition of a single atom.[2,3] Here, we show that finite size effects can give rise to a significant magnetic moment in a Cu nanocluster leading to magnetization-dependent reactivity; this dependence on magnetization could be a path to magnetic control of catalytic activity.

We focus on selective hydrogenation on Cu, which is non-magnetic in its bulk form. The reason for our choice is that the surfaces of bulk Cu exhibit high selectivity for industrially important reactions, but they require elevated temperatures and pressures to compensate for their poor H_2 dissociation kinetics.[4,5] While improvements have been proposed for bulk surfaces, such as the use of dilute alloys,[5] the possibility of using Cu nanoclusters has been less explored. Previous surveys of gas phase cluster reactivity[6,7] investigated D_2 interactions with small Cu nanoclusters but found no evidence of dissociative chemisorption at temperatures near 300 K and effective D_2 pressures below 50 Torr. Gas phase cluster reactivity exhibits mechanism-dependent temperature and pressure effects,[3] however, so different experimental conditions might yield measureable activity. We return to these pressure and temperature considerations later in light of our results.

We investigated H_2 dissociation on an icosahedral nanocluster of Cu using first-principles density functional theory (DFT) calculations with the SIESTA[8] code (see SI for details). Early studies using empirical interatomic potentials found icosahedral geometries to be most

stable, but more recent work using first-principles quantum chemistry methods predict disordered minimum-energy geometries for Cu_{13} and other 13-atom fcc metal clusters.[9,10] Nevertheless, icosahedral Cu_{13} can be synthesized in solution using synchrotron radiolysis.[11] Electrochemical Cu_{13} synthesis has also been reported,[12] with sizes consistent with an icosahedral geometry, but the structure could not be determined precisely. More importantly, the 3-fold hollow sites of icosahedral Cu_{13} are locally identical to hcp hollow sites on the well-studied bulk Cu(111) surface; this similarity in structural features can reveal finite size effects with greater clarity.

Icosahedral Cu_{13} nanoclusters have a significantly different electronic structure than Cu(111) surfaces. Quantum size effects produce discrete energy levels while the icosahedral symmetry yields 5-fold degeneracies in both spin directions to produce 10 total valence states. The five valence electrons of Cu_{13} then follow Hund's rule to fully occupy the five majority-spin states and leave the minority-spin states unoccupied. The result is a large ground-state magnetization of $5\,\mu_B$, as noted previously,[13] and an exchange splitting of 0.47 eV, as shown in Figure 1. Other 13-atom metal nanoclusters, either of icosahedral shape or with different structure, are also predicted to have significant magnetization, including Ni_{13}, Ag_{13}, and Au_{13}.[10,13,14] This appears to be a general trend in nanoclusters, where the discrete densities of states combine with symmetry-induced multiple degeneracy to produce net magnetization through exchange splitting.[14]

In contrast to bulk Cu and other transition metal surfaces, H_2 molecules can adsorb weakly on Cu_{13} intact. There are two nearly isoenergetic geometries: one with a net magnetization of $5\,\mu_B$ and H–Cu bonds of length 1.90 Å, and another with $3\,\mu_B$ and H–Cu bonds of length 1.73 Å. The geometries are qualitatively similar, with the H–H bond axis centered above an apex Cu atom. The geometry with shorter bonds, shown in Figure 2, is marginally more stable with total energy lower by 0.04 eV. Qualitatively similar changes in magnetization upon exposure to hydrogen have been experimentally observed for thin films[15] and nanoislands.[16] The magnetization reduction in Cu_{13} is caused by the shorter H–Cu bonds

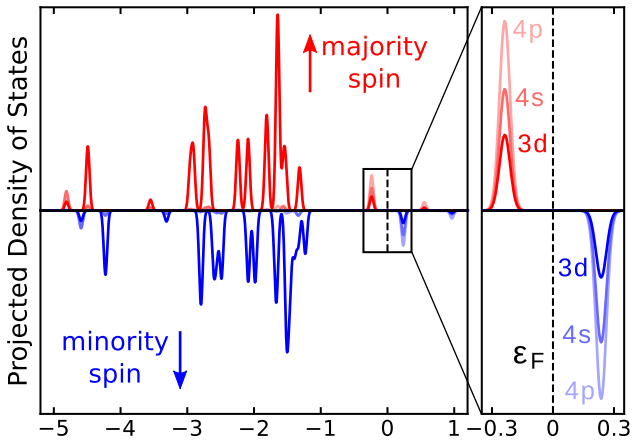

Figure 1: Spin-resolved projected density of states near the Fermi level of the icosahedral Cu_{13} nanocluster for the majority (up, red) and the minority (down, blue) spin components. Contributions from different orbitals are identified for both spin directions.

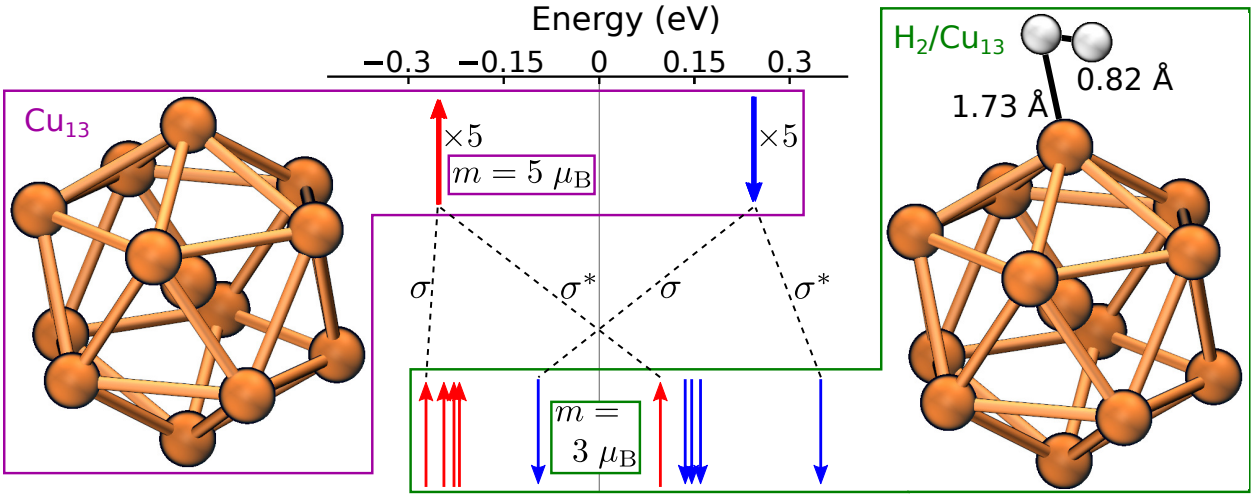

Figure 2: Illustration of how H-Cu hybridization drives the magnetization switch. Structural figures show the clean cluster (left, purple box) and the one with H_2 adsorbed (right, green box).

and increased hybridization with Cu orbitals, which pushes the energy of the antibonding majority-spin state above that of the bonding minority-spin state. The mechansim is illustrated in Figure 2, the inversion of spin states produces the observed magnetization change by $-2\,\mu_B$. Despite its greater stability, the lower magnetization geometry only has a weak adsorption energy of 0.09 eV, such that H_2 dissociation will most likely proceed from molecular collisions with Cu_{13} rather than thermal activation. The same is true of bulk Cu surfaces.[17]

The initial magnetization of $5\,\mu_B$ for isolated Cu_{13} differs from the magnetization of $3\,\mu_B$ for the H_2/Cu_{13} complex, but the weak spin-orbit coupling of both H and Cu means that the magnetization switch required for adiabatic dissociation may not actually take place. We therefore obtain transition states and reaction pathways for a fixed magnetization state of $3\,\mu_B$ and $5\,\mu_B$ separately. Figure 3 shows the minimum-energy pathway for H_2 dissociation: H_2 first slides parallel to a Cu–Cu bridge (green to white), followed by bond cleavage and relaxation to the nearest local minimum (white to purple). The dissociated final state has one H atom at a hollow site and the other adsorbed at a Cu–Cu bridge site, the second-nearest bridge for the low magnetization structure and the third-nearest bridge for the high magnetization structure. In contrast to the smooth minimum-energy pathway on the Cu(111) surface, the minimum-energy pathways on Cu_{13} for both magnetization states have two major high-curvature regions: one for the right-most H atom at the point of H_2 dissociation, and another for the left-most H atom during the subsequent descent to the final state.

The activation energy for H_2 dissociation is quite different in the two magnetization states: 0.20 eV in the low magnetization state and 0.67 eV in the high magnetization state. This dependence on magnetization is caused by increasingly large bonding-antibonding splitting along the minimum-energy pathway. In the adiabatic case, which involves a switch in magnetization from $5\,\mu_B$ to $3\,\mu_B$, the high-energy antibonding state becomes unoccupied in favor of the lower-energy bonding state of opposite spin. The resulting activation energy is relatively small at 0.20 eV. In the limit of no spin-orbit coupling, however, the high-energy antibonding state remains occupied and the transition state is higher by 0.47 eV. In compari-

son, the Cu(111) and Cu(110) surfaces have activation energies around 0.4 eV to 0.5 eV[4,17,18] depending on the experimental or computational method used to estimate their value. Since the low magnetization and high magnetization activation energies on Cu_{13} differ significantly, and straddle those of bulk Cu surfaces, we conclude that H_2 dissociation rates may depend critically on the probability of a magnetization switch.

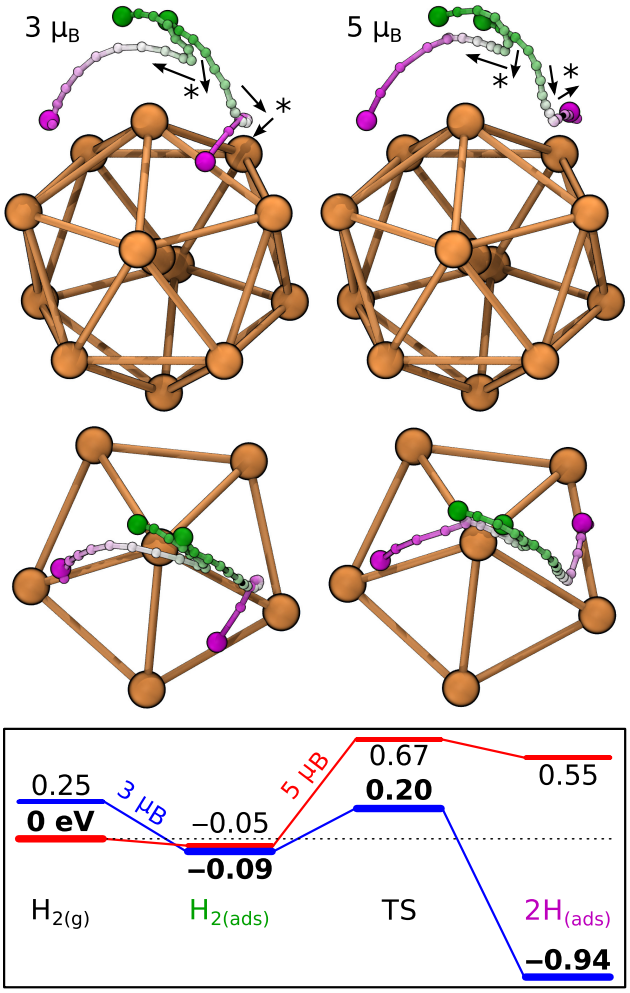

Figure 3: Top: minimum-energy pathways for H_2 dissociation at fixed magnetization of $3\,\mu_B$ and $5\,\mu_B$. The green-white-purple gradient indicates reaction progress, with the initial and final states indicated by larger spheres. High curvature regions are marked with $*$. Bottom: energy of key intermediates, with the adiabatic ground-state energy in bold; the zero of energy is defined as the energy of the isolated H_2 and Cu_{13} at $5\,\mu_B$.

To estimate this probability we ran 100 Born-Oppenheimer (BO) molecular dynamics simulations to obtain typical dissociation trajectories along the adiabatic potential energy

surface. To ensure that each trajectory corresponds to H_2 dissociation, we start the simulation at the transition state geometry and run time backward to the associated state. Initial H_2 kinetic energies ranged from 0.05 to 0.40 eV, and velocity directions were chosen randomly. Since adiabatic dynamics are time-reversible, these initial conditions randomly sample H_2-Cu_{13} collisions which result in H_2 dissociation. The time-dependent magnetization for each trajectory exhibits the adiabatic magnetization switch from $3\,\mu_B$ to $5\,\mu_B$ as the H atoms recombine, involving the inversion of opposite-spin Kohn-Sham states shown in Figure 2. Analyzing each trajectory can then produce an estimate of the probability P_{LZ} of a magnetization switch using the Landau-Zener approximation (see SI for details):

$$P_{LZ} = 1 - \exp\left(-2\pi\Gamma\right), \quad \Gamma \equiv \frac{\delta^2/\hbar}{\left|\frac{\partial}{\partial t}\left(E_h(t) - E_l(t)\right)\right|} \tag{1}$$

where $E_h(t)$ and $E_l(t)$ are the potential energies at high magnetization ($5\,\mu_B$) and low magnetization ($3\,\mu_B$), respectively, and $\delta = 8.15$ meV is the experimentally observed Rashba splitting for the Cu(111) surface.[19] The spin-orbit splitting can be estimated from first-principles using the DFT spin-orbit coupling Hamiltonian[20] ($\delta \approx 12$ meV, see SI), but previous DFT calculations significantly overestimated the Cu(111) Rashba splitting[19] so we use the experimental value instead. Each randomized trajectory samples the denominator in the expression for Γ in eq 1 (see SI). P_{LZ} varies significantly with H_2 center of mass (CM) velocities away from Cu_{13} at the avoided crossing as shown in Figure 4. The fitting equation is derived by approximating the denominator of Γ, the crossing rate, as the CM velocity v_{CM} away from the nanocluster multiplied by a scalar constant g, which is fitted to the data. Overall the median probability and interquartile range for P_{LZ} is $(6.2 \pm 1.4)\,\%$. Adiabatic transition state theory therefore overestimates reaction rates by a factor of $1/P_{LZ} \approx 16$.

Since the weak spin-orbit coupling of Cu and H hinders the magnetization switch and hence reduces reaction rates, we now discuss several methods for improving the performance of Cu_{13} as a H_2 dissociation catalyst. One approach is to excite nanoclusters to the lower

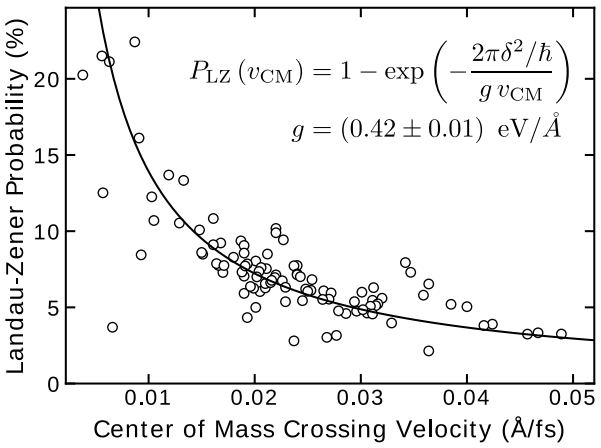

Figure 4: Landau-Zener probabilities P_{LZ} versus the H_2 center of mass velocity v_{CM} away from Cu_{13}. Open circles show results calculated from the 100 adiabatic molecular dynamics trajectories. The minimum mean absolute error fit of the Landau-Zener formula is indicated by the solid line.

magnetization state in advance of a H_2-Cu_{13} collision. Such excitations would bypass the hindered magnetization switch and decrease activation energies by destabilizing the isolated nanocluster. Defining ΔE_{TS} to be the activation energy for H_2 dissociation relative to isolated H_2 and Cu_{13}, we use $\Delta E_{\mathrm{TS}}^{\mathrm{BO}}$ to refer to the Born-Oppenheimer limit where the system remains in its electronic ground state, and $\Delta E_{\mathrm{TS}}^{*}$ to refer to the excited initial state. Both values are shown for Cu_{13} and other clusters (discussed below) in Table 1. While $\Delta E_{\mathrm{TS}}^{\mathrm{BO}}$ is 0.20 eV, $\Delta E_{\mathrm{TS}}^{*}$ is negative so H_2 can dissociate over magnetically excited Cu_{13} at arbitrarily slow collision velocities. These excitations could be induced using optical spin-flips and intense irradiation to compensate for the weak spin-orbit coupling of Cu.[21] Since the density of states is discrete near the Fermi level for both spin directions, the incident optical spectrum could be tuned to a narrow band around the exchange splitting of 0.47 eV ($\lambda \approx 2.7$ μm) to specifically target the spin-flip excitation.

Another approach for improving catalytic rates is to modify the electronic structure of Cu_{13} so that a magnetization switch is no longer needed. The high activation energy for the high magnetization state is caused by occupying the highest antibonding state as shown in Figure 2. Depopulating this state using electron deficient clusters should result in activation

energies that vary less with magnetization. To address this possibility, we consider electron deficient Cu clusters, Cu_{13}^+, or clusters formed by substitution of a surface Cu atom by an atom with fewer valence electrons, $Cu_{12}Ni$ and $Cu_{12}Pd$. Isolated Pd atoms in particular have been shown to facilitate H_2 dissociation on bulk Cu surfaces.[5,22] All three electron-deficient clusters we considered have magnetization of $4\,\mu_B$ in their ground state since one of the majority-spin antibonding states is no longer occupied. To investigate the effect of Ni and Pd substitution without changing the number of valence electrons, we also consider $Cu_{12}Ni^-$ and $Cu_{12}Pd^-$ anions with five valence electrons and ground-state magnetization of $5\,\mu_B$. All clusters have nearly icosahedral geometries and similar densities of states near the Fermi level.

Table 1: Magnetization of the Isolated (m_I) and Adsorbed ($m_{\mathbf{ads}}$) H_2/Nanocluster Systems, Adsorption Energy $E_{\mathbf{ads}}$, and Activation Energies Relative to the Gas Phase ($\Delta E_{\mathbf{TS}}$) and Adsorbed H_2 ($\Delta E_{\mathbf{A}}$)

Cluster	m_I	m_{ads}	E_{ads}	$\Delta E_{\mathrm{TS}}^{\delta\to 0}$	$\Delta E_{\mathrm{TS}}^{\mathrm{BO}}$	$\Delta E_{\mathrm{TS}}^{*}$	$\Delta E_{\mathrm{A}}^{\delta\to 0}$	$\Delta E_{\mathrm{A}}^{\mathrm{BO}}$
Cu_{13}	5	3	0.09	0.67	0.20	−0.05	0.72	0.29
Cu_{13}^+	4	4	0.34	0.29	0.10	−0.11	0.63	0.43
$Cu_{12}Ni$	4	4	0.77	−0.54	−0.58	−0.71	0.23	0.18
$Cu_{12}Ni^-$	5	3	0.69	−0.33	−0.60	−0.81	0.20	0.08
$Cu_{12}Pd$	4	4	0.53	−0.16	−0.19	−0.27	0.38	0.35
$Cu_{12}Pd^-$	5	3	0.47	−0.06	−0.30	−0.43	0.34	0.17

Energies are in eV, and magnetization values are in μ_B.

Table 1 summarizes the energetics of H_2 dissociation on all six nanoclusters we considered. H_2 adsorption only induces magnetization switches for clusters with five valence electrons (Cu_{13}, $Cu_{12}Ni^-$, and $Cu_{12}Pd^-$). However, as H–Cu hybridization increases along the minimum-energy pathway, clusters with ground state magnetization of $4\,\mu_B$ undergo a corresponding switch from $4\,\mu_B$ to $2\,\mu_B$ before reaching the transition state. Therefore the transition states for all six clusters have lower magnetization than their corresponding ground states by $2\,\mu_B$. Similar to bulk Cu surfaces, Ni and Pd dopants increase the H_2 adsorption energy while reducing the activation energy; all four clusters with substituted Cu atoms have lower activation energy than desorption energy so H_2 dissociation can pro-

ceed from both thermal activation and gas phase collisions. To distinguish between these possibilities, we use ΔE_{A} for activation energy relative to the adsorbed state, and ΔE_{TS} for the activation energy relative to isolated H_2 and the nanocluster. Superscripts indicate the relevant magnetic limits: $\delta \to 0$ for the zero spin-orbit coupling limit, and BO for the adiabatic limit following the Born-Oppenheimer approximation. $Cu_{12}Ni$ and $Cu_{12}Ni^-$ have the lowest activation energy regardless of the magnetization state.

As expected, electron-deficient clusters exhibit smaller changes in ΔE_{A} and ΔE_{TS} with respect to magnetization (see Table 1). For example, $\Delta E_{\mathrm{TS}}^{\delta\to 0} - \Delta E_{\mathrm{TS}}^{\mathrm{BO}}$ is 0.47 eV for Cu_{13}, but only 0.19 eV for Cu_{13}^+. The adiabatic activation energy for all clusters is lower than the $\delta \to 0$ "fixed magnetization" limit, so adiabatic transition state theory overestimates H_2 dissociation rates for all six clusters. Magnetization differences in ΔE_{TS} are most important for Cu_{13} and Cu_{13}^+ where H_2 dissociation mostly proceeds from collisions, while differences in ΔE_{A} are more important for clusters with substituted Cu atoms where thermally activated H_2 dissociation is likely.

Finally, we consider using co-catalysts to improve the performance of Cu_{13} in H_2 dissociation. One particularly simple strategy is to consider H_2 as its own co-catalyst: H_2 adsorption can induce the hindered magnetization switch for the dissociation of a subsequent H_2 molecule. This approach is feasible since H_2 grows more stable with increasing coverage. The adsorption and activation energy for increasing H_2 coverages is shown in Table 2, where $E_{\mathrm{ads}}^{(k)}$ is the incremental adsorption energy of the k^{th} H_2 molecule on $(k-1)H_2/Cu_{13}$. $2H_2/Cu_{13}$ has the highest incremental adsorption energy and should therefore be the most common complex at equilibrium. Adsorption and transition-state geometries still have ground-state magnetization of $3\,\mu_{\mathrm{B}}$ except for H_2 dissociating over the $2H_2/Cu_{13}$ complex, where the magnetization is $1\,\mu_{\mathrm{B}}$ due to further increases in H-Cu hybridization. We also find that the most common $2H_2/Cu_{13}$ arrangement produces the lowest $\Delta E_{\mathrm{TS}}^{\mathrm{BO}}$ value of only 0.01 eV. Although a switch from $3\,\mu_{\mathrm{B}}$ to $1\,\mu_{\mathrm{B}}$ becomes necessary, the corresponding P_{LZ} is likely more than offset by the large 0.2 eV decrease in the activation energy. This signficant decrease

in activation energy with coverage suggests that hydrogen dissociation might be observed experimentally on Cu_{13} nanoclusters using a combination of low temperatures, improving the stability of weakly adsorbed H_2 molecules,[3] and high H_2 pressures. In contrast, previous experimental work[6,7] may not have observed D_2-Cu_{13} interactions due to using low pressures (below 50 Torr) and high temperatures (near 300 K) relative to the adsorption energy of H_2.

Table 2: Incremental Adsorption Energies $E_{\mathbf{ads}}^{(k)}$ and Activation Energies $\Delta E_{\mathbf{TS}}^{(k)}$ for Multiple H_2 Adsorption on Cu_{13}

k	$E_{\mathrm{ads}}^{(k)}$	$\Delta E_{\mathrm{TS}}^{(k),\delta\to 0}$	$\Delta E_{\mathrm{TS}}^{(k),\mathrm{BO}}$
1	0.09	0.67	0.20
2	**0.30**	0.21	0.21
3	0.15	**0.23**	**0.01**

Energies are in eV, and the most stable arrangement and most common ΔE_{TS} values are shown in bold.

In conclusion, we investigated the catalytic behavior of Cu_{13} clusters for H_2 dissociation and demonstrated that magnetization and spin-orbit coupling play an important role in this reaction. A combination of high symmetry in the cluster geometry and quantum size effects give Cu_{13} a large magnetic moment leading to magnetization-dependent catalytic behavior. The most favorable reaction pathway requires a magnetization switch, which is hindered by the weak spin-orbit coupling of H and Cu. The corresponding probability $P_{\mathrm{LZ}} \approx 6.2\%$ of a magnetization switch means that adiabatic transition state theory overestimates reaction rates for the H_2/Cu_{13} system by a factor of $1/P_{\mathrm{LZ}} \approx 16$. Therefore magnetization presents a new challenge for designing nanoscale catalysts for H_2 dissociation and hydrogenation. This magnetization dependence also offers new opportunities to control catalyst behavior by changing magnetic states. For example, ground-state Cu_{13} features a substantial collisional activation energy of 0.20 eV, but we predict that excited Cu_{13} which has lower magnetization will facilitate H_2 dissociation at arbitrarily slow collision velocities. The magnetization switch could be induced by optical spin-flip excitations. Appropriately designed catalysts with controllable magnetization, for example using optical or magnetic fields, could provide new ways to control catalyst activity without altering more conventional reaction parameters

such as temperature, pressure, and reactant composition.

Acknowledgement

This work was supported by Integrated Mesoscale Architectures for Sustainable Catalysis, an Energy Frontier Research Center funded the U.S. Department of Energy, Office of Science, Basic Sciences under Award No. DESC0012573. Calculations were performed on the Odyssey cluster supported by the FAS Division of Science, Research Computing Group at Harvard University. We thank Professor Jaime Ferrer for providing a version of the SIESTA package with spin-orbit coupling.

Supporting Information Available

Details of DFT calculations and estimating probabilities of magnetization switches

This material is available free of charge via the Internet at `http://pubs.acs.org/`.

References

(1) Wilcoxon, J. P.; Abrams, B. L. Synthesis, Structure and Properties of Metal Nanoclusters. *Chem. Soc. Rev.* **2006**, *35* (11), 1162–1194.

(2) Crampton, A. S.; Rötzer, M. D.; Ridge, C. J.; Schweinberger, F. F.; Heiz, U.; Yoon, B.; Landman, U. Structure Sensitivity in the Nonscalable Regime Explored via Catalysed Ethylene Hydrogenation on Supported Platinum Nanoclusters. *Nat. Commun.* **2016**, *7*, 10389.

(3) Knickelbein, M. B. Reactions of Transition Metal Clusters with Small Molecules. *Annu. Rev. Phys. Chem.* **1999**, *50* (1), 79–115.

(4) Hammer, B.; Nørskov, J. K. Why Gold is the Noblest of All the Metals. *Nature* **1995**, *376*, 238–240.

(5) Kyriakou, G.; Boucher, M. B.; Jewell, A. D.; Lewis, E. A.; Lawton, T. J.; Baber, A. E.; Tierney, H. L.; Flytzani-Stephanopoulos, M.; Sykes, E. C. H. Isolated Metal Atom Geometries as a Strategy for Selective Heterogeneous Hydrogenations. *Science* **2012**, *335* (6073), 1209–1212.

(6) Morse, M. D.; Geusic, M. E.; Heath, J. R.; Smalley, R. E. Surface Reactions of Metal Clusters. II. Reactivity Surveys with D_2, N_2, and CO. *J. Chem. Phys.* **1985**, *83* (5), 2293–2304.

(7) Andersson, M.; Persson, J. L.; Rosén, A. Reactivity of Fe_n, Co_n, and Cu_n Clusters with O_2 and D_2 Studied at Single-Collision Conditions. *J. Phys. Chem.* **1996**, *100* (30), 12222–12234.

(8) Soler, J. M.; Artacho, E.; Gale, J. D.; García, A.; Junquera, J.; Ordejón, P.; Sánchez-Portal, D. The SIESTA Method for Ab Initio Order-N Materials Simulation. *J. Phys.: Condens. Matter* **2002**, *14* (11), 2745–2779.

(9) Oviedo, J.; Palmer, R. E. Amorphous Structures of Cu, Ag, and Au Nanoclusters from First Principles Calculations. *J. Chem. Phys.* **2002**, *117* (21), 9548–9551.

(10) Chou, J. P.; Hsing, C. R.; Wei, C. M.; Cheng, C.; Chang, C. M. Ab Initio Random Structure Search for 13-Atom Clusters of fcc Elements. *J. Phys.: Condens. Matter* **2013**, *25* (12), 125305.

(11) Oyanagi, H.; Orimoto, Y.; Hayakawa, K.; Hatada, K.; Sun, Z.; Zhang, L.; Yamashita, K.; Nakamura, H.; Uehara, M.; Fukano, A. et al. Nanoclusters Synthesized by Synchrotron Radiolysis in Concert with Wet Chemistry. *Sci. Rep.* **2014**, *4*, 7199.

(12) Vilar-Vidal, N.; Rivas, J.; López-Quintela, M. A. Size Dependent Catalytic Activity of Reusable Subnanometer Copper(0) Clusters. *ACS Catal.* **2012**, *2* (8), 1693–1697.

(13) Longo, R. C.; Gallego, L. J. Structures of 13-Atom Clusters of fcc Transition Metals by Ab Initio and Semiempirical Calculations. *Phys. Rev. B* **2006**, *74* (19), 193409.

(14) Luo, W.; Pennycook, S. J.; Pantelides, S. T. s-Electron Ferromagnetism in Gold and Silver Nanoclusters. *Nano Lett.* **2007**, *7* (10), 3134–3137.

(15) Lin, W.-C.; Tsai, C.-J.; Huang, H.-Y.; Wang, B.-Y.; Mudinepalli, V. R.; Chiu, H.-C. Hydrogen-Mediated Long-Range Magnetic Ordering in Pd-Rich Alloy Film. *Appl. Phys. Lett.* **2015**, *106* (1), 012404.

(16) Park, J.; Park, C.; Yoon, M.; Li, A.-P. Surface Magnetism of Cobalt Nanoislands Controlled by Atomic Hydrogen. *Nano Lett.* **2017**, *17* (1), 292–298.

(17) Rendulic, K.; Winkler, A. Adsorption and Desorption Dynamics as Seen Through Molecular Beam Techniques. *Surf. Sci.* **1994**, *299-300*, 261–276.

(18) Mills, G.; Jónsson, H.; Schenter, G. K. Reversible Work Transition State Theory: Application to Dissociative Adsorption of Hydrogen. *Surf. Sci.* **1995**, *324* (2), 305–337.

(19) Tamai, A.; Meevasana, W.; King, P. D. C.; Nicholson, C. W.; de la Torre, A.; Rozbicki, E.; Baumberger, F. Spin-Orbit Splitting of the Shockley Surface State on Cu(111). *Phys. Rev. B* **2013**, *87* (7), 075113.

(20) Fernández-Seivane, L.; Oliveira, M. A.; Sanvito, S.; Ferrer, J. On-Site Approximation for Spin-Orbit Coupling in Linear Combination of Atomic Orbitals Density Functional Methods. *J. Phys. Condens. Matter* **2007**, *19* (48), 489001.

(21) Ibañez-Azpiroz, J.; Eiguren, A.; Sherman, E. Y.; Bergara, A. Spin-Flip Transitions Induced by Time-Dependent Electric Fields in Surfaces with Strong Spin-Orbit Interaction. *Phys. Rev. Lett.* **2012**, *109* (15), 156401.

(22) Fu, Q.; Luo, Y. Catalytic Activity of Single Transition-Metal Atom Doped in Cu(111)

Surface for Heterogeneous Hydrogenation. *J. Phys. Chem. C* **2013**, *117* (28), 14618–14624.